Chapter 5

A Method of Evaluating the Presence of Fan-Blade-Rotation Induced Unsteadiness in Wind Tunnel Experiments

Josué Njock Libii

Additional information is available at the end of the chapter

http://dx.doi.org/10.5772/54144

1. Introduction

1.1. Flows driven by a constant pressure gradient through a pipe of circular cross section

When the flow of a Newtonian fluid in a pipe of circular cross section is driven solely by a constant pressure gradient, the resulting velocity distribution is a quadratic function of the radial distance from the axis of the pipe. The velocity profile of such a flow has, therefore, a parabolic distribution in which the maximum velocity occurs on the axis of the pipe. A graphical representation of this type of velocity is shown in Figure 1.

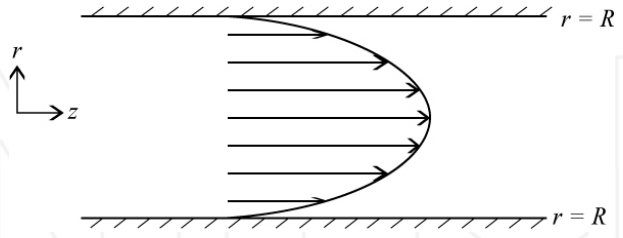

Figure 1. The parabolic velocity profile for flow driven by a constant pressure gradient in a circular pipe

1.2. Flows driven by a sinusoidal pressure gradient through a pipe of circular cross section

Things become more complicated if the pressure gradient varies with time. When, for example, the pressure gradient fluctuates with time in such a way that that gradient can be ex-

pressed as a simple sinusoidal function, the velocity profile remains parabolic only at very low frequencies of fluctuation. At very high frequencies, the location of the maximum velocity moves away from the axis of the pipe and towards the wall. The higher the frequency of oscillations of the pressure gradient, the farther away the point of maximum velocity moves from the axis of the pipe. Sample plots of velocity profiles that were generated at high frequencies of fluctuations are shown in the literature by Uchida (1956). Here, Figure 2 is one such example, where five snapshots of velocity profiles at different times are displayed, from left to right, within one complete cycle: at the beginning, one-quarter, half-way, three-quarters of the way, and at the very end of the cycle. The values of the parameters that were used to generate these plots are summarized below:

$$-\frac{1}{\rho K}\frac{\partial p}{\partial x}=\cos(nt);\quad k=\sqrt{\frac{n}{v}}R=5;c=\frac{Kk^2}{8n}=3.125\frac{K}{n}$$

Where n is the circular frequency, p the pressure, ρ the mass density of the fluid, t the time, x the axial coordinate, R the inside radius of the pipe, u the axial speed of the fluid, v the coefficient of kinematic viscosity, k a dimensionless ratio used by Schlichting to denote the magnitude of the frequency of oscillation, and K is a constant that indicates the size of the pressure gradient.

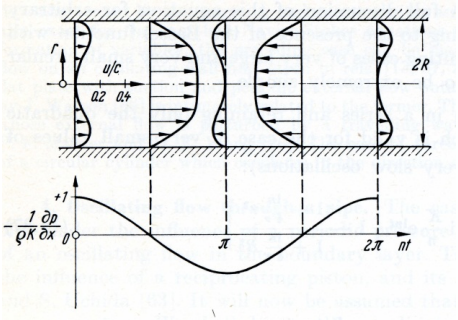

Figure 2. Sample velocity profiles for flow driven by a sinusoidal pressure gradient in a circular pipe [Uchida]

1.3. The mean velocity squared and Richardson's annular effect

The higher the frequency of oscillations of the pressure gradient, the farther away the point of maximum velocity moves from the axis of the pipe. The phenomenon in which the point of maximum velocity moves away from the axis of the pipe and shifts towards its wall is known as Richardson's annular effect. It was demonstrated experimentally by Richardson (1929), proved analytically by Sexl (1930), and demonstrated to hold for any pressure gradient that is periodic with time by Uchida (1956).

When the sinusoidal pressure gradient that drives the flow in a circular pipe has fast oscillations, the mean velocity squared computed with respect to time is found to be

http://dx.doi.org/10.5772/54144

$$\overline{u^2(r)} = \frac{K^2}{2n^2}\left\{1 - 2\sqrt{\frac{R}{r}}\exp\left[-\sqrt{\frac{n}{2v}}(R-r)\right]\cos\left[\sqrt{\frac{n}{2v}}(R-r)\right] + \frac{R}{r}\exp\left[-2\sqrt{\frac{n}{2v}}(R-r)\right]\right\} \quad (1)$$

Where r is the radial distance from the axis of the pipe; and letting $y = (R - r)$ be a new variable that represents the distance from the wall of that pipe, a dimensionless distance from that wall can be defined as $\eta = y\sqrt{\frac{n}{2v}}$. Using this distance, one can nondimensionalize the mean velocity squared as shown below :

$$\frac{\overline{u^2(r)}}{\left(\frac{K^2}{2n^2}\right)} = \left\{1 - 2\sqrt{\frac{R}{r}}\exp\left[-\sqrt{\frac{n}{2v}}(R-r)\right]\cos\left[\sqrt{\frac{n}{2v}}(R-r)\right] + \frac{R}{r}\exp\left[-2\sqrt{\frac{n}{2v}}(R-r)\right]\right\} \quad (2)$$

When one is very close to the wall of the pipe, r and R are very close in magnitude and $\frac{R}{r} \approx 1$. This causes the expression in Eq. (2) to become

$$\frac{\overline{u^2(y)}}{\left(\frac{K^2}{2n^2}\right)} = 1 - 2\exp(-\eta)\cos\eta + \exp(-2\eta). \quad (3)$$

When the variation of the expression of the mean velocity squared in Eq. (3) is plotted against the dimensionless distance η, as shown in Figure 3, one can see that the location of the maximum velocity is not on the axis of the pipe as is the case in steady flow and at very low oscillations of the pressure gradient. Instead, it occurs near the wall of the pipe at a dimensionless distance $\eta = y\sqrt{\frac{n}{2v}} = 2.28$. This value has been shown to agree with experimental data collected by Richardson (1929).

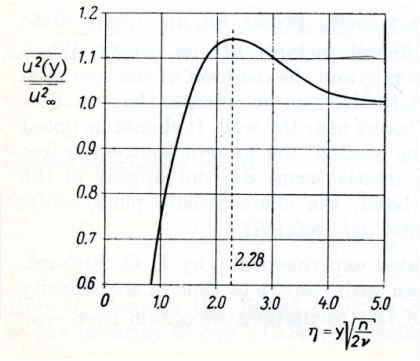

Figure 3. Variation of the mean with respect to time of the velocity squared for periodic pipe flows that are very fast

In this Figure 3, y is the distance from the wall of the pipe and $u_\infty^2 = \frac{K^2}{2n^2}$ *represents* the mean with respect to time of the velocity squared at a large distance from the wall.

2. Richardson's annular effect in a wind tunnel

Unsteady pulsating flows occur in many situations that have a practical engineering importance. These include high- speed pulsating flows in reciprocating piston-driven flows, rotor blade aerodynamics and turbomachinery. They also arise in wind-tunnel flows. When the velocity distribution is measured across the test section of a subsonic wind tunnel that is driven by a high speed fan, it has been observed experimentally that, in addition to the effect of the boundary layer that is expected near the wall, Richardson's annular effect can be demonstrated as well. Indeed, published experimental results from our laboratory have demonstrated that Richardson's annular effect can occur in a wind tunnel (Njock Libii, 2011).

The purpose of the remainder of this chapter is to summarize the theoretical basis of the Richardson's annular effect in pipes of circular sections and in rectangular tubes, illustrate its results graphically, and relate them to what happens in a wind tunnel.

First Stokes' second problem is reviewed briefly. The theory of pulsating flows in pipes and ducts is summarized. The anatomy of the shift in the location of the maximum velocity from the center to points near the wall is presented using series approximations and graphical illustrations.

3. Stokes' second problem

Fundamental studies of fully-developed and periodic pipe and duct flows with pressure gradients that vary sinusoidally have been done (Sexl, 1930). From such studies, we know that, when an incompressible and viscous fluid is forced to move under a pulsating pressure difference in a pipe or a duct, some characteristic features are always observed. Some of these features are similar to those that are observed to occur in the boundary layer adjacent to a body that is performing reciprocating harmonic oscillations. These features are related to the results of a classic problem solved by Stokes, known as Stokes' second problem, which gives details of the behavior of the boundary layer in a viscous fluid of kinematic viscosity, v, that is bounded by an infinite plane surface that moves back and forth in its own plane with a simple harmonic oscillation that has a circular frequency, ω.

Stokes solution shows that, for this type of flow, 1) transverse waves propagate away from the oscillating surface and into the viscous fluid; 2) the direction of the velocity of these waves is perpendicular to the direction of propagation; 3) the oscillating fluid layer so generated has a phase lag, φ, with respect to the motion of the wall; and 4) that phase lag, which varies with y, the distance from the wall, is given by, $\varphi = \frac{y}{\delta}$, where δ represents a length scale introduced by Stokes; that length, called the depth of penetration of the wave into the fluid, is given by $\delta = \left(\frac{2v}{\omega}\right)^{1/2}$. The thickness of the boundary layer is proportional to the penetration depth, δ. The value of the constant of proportionality varies with the point

http://dx.doi.org/10.5772/54144

that one designates to be the edge of the boundary layer. Thus, For example, if one defines the edge of the boundary layer to be the point in the flow where the speed inside the boundary layer become equal to 99% of the speed of flow outside the boundary layer, the constant of proportionality is 4.6. Then, the thickness of the boundary layer at that point is equal to 4.6 δ.

4. Pulsating flow through pipes

4.1. Basic equations

The flow of a viscous fluid in a straight pipe of circular cross-section due to a periodic pressure gradient was examined experimentally and theoretically by Richardson and Tyler (1929) and theoretically by Sexl (1930). If the pipe is sufficiently long, variations of flow parameters along its axis may be neglected and the only component of flow is that along the axis of the pipe. The Navier-Stokes equations become

$$\frac{\partial u}{\partial t} = -\frac{1}{\rho}\frac{\partial p}{\partial x} + \nu\left(\frac{\partial^2 u}{\partial r^2} + \frac{1}{r}\frac{\partial u}{\partial r}\right) \tag{4}$$

$u(r=a,\ t)=0$; *and* $u(r=0,\ t)=$ *finite*

$$-\frac{1}{\rho}\frac{\partial p}{\partial x} = a\ function\ of\ time \tag{5}$$

Where u = u(r, t) is the component of velocity in the axial direction x, $\frac{\partial p}{\partial x}$ is the pressure gradient in the axial direction, t is the time, v is the kinematic viscosity of the fluid, r is the radial distance measured from the axis of the pipe, and a is the inside radius of the pipe. For a given pressure gradient, one seeks solutions that are finite at r = 0 and satisfy the no-slip condition u = 0 on the wall of the pipe at all times. We present two cases: First, the case of a sinusoidal pressure gradient that was first solved by Sexl (1930) and then that of a general periodic pressure gradient that was first solved by Uchida (1956).

4.2. Case of a sinusoidal pressure gradient: Sexl's method (1930)

If the pressure gradient is sinusoidal and given the form

$$\frac{\partial p}{\partial x} = \rho C cos(\omega t), \tag{6}$$

then, the solution is given by the real part of

$$u(r,\ t) = -i\frac{C}{\omega}\left\{1 - \frac{J_o\left((-ix)^{\frac{1}{2}}\frac{r}{a}\right)}{J_o\left((-ix)^{\frac{1}{2}}\right)}\right\}e^{i\omega t} \tag{7}$$

Where J_o is the Bessel function of the first kind and of zero order (Watson,1944) and, here, x is defined as shown below:

$$x = \frac{\omega a^2}{v}. \tag{8}$$

For small values of the parameter x, the real part of the velocity u can be written as

$$u(r,\ t) = \frac{C}{4v}\left(a^2 - r^2\right)\cos(\omega t) \tag{9}$$

and for large values of the parameter x and of $\left(\frac{r}{a}\right)^2$, the velocity can be represented by

$$u(r,\ t) = \frac{C}{\omega}\left\{\sin(\omega t) - \left(\frac{a}{r}\right)^{1/2}\exp(-\alpha)\sin[\omega t - \alpha]\right\}; \tag{10}$$

where

$$\alpha = \left(\frac{x}{2}\right)^{1/2}\left(1 - \frac{r}{a}\right). \tag{11}$$

Furthermore, the mean velocity squared computed with respect to time is found to be

$$\overline{u^2(r)} = \frac{C^2}{2\omega^2}\left\{1 - 2\left(\frac{a}{r}\right)^{\frac{1}{2}}\exp(-\alpha)\cos(\alpha) + \left(\frac{a}{r}\right)\exp(-2\alpha)\right\}. \tag{12}$$

These well-known results indicate that the representation of the velocity changes radically as one varies the parameter x from very small to very large values. For example, the maximum velocity reaches its maximum amplitude on the axis of the pipe when x is very small. However, when the frequency of fluctuations becomes large, the location of the maximum velocity shifts away from the axis of the pipe and moves closer and closer to the wall of the pipe as the parameter increases, Fig. 4. Indeed, in the latter case, the expression for the location of maximum velocity is given by

$$r = a\left(1 - 3.22x^{-1/2}\right). \tag{13}$$

http://dx.doi.org/10.5772/54144

4.3. Case of a general periodic pressure gradient: Uchida's general theory

The case of a general periodic pressure gradient was solved by Uchida (1956), whose solution is summarized below.

Consider a general periodic function that can be expressed using a Fourier series as follows:

$$-\frac{1}{\varrho}\frac{\partial p}{\partial x} = \varkappa_0 + \sum_{n=1}^{\infty} \varkappa_{cn} \cos nt + \sum_{n=1}^{\infty} \varkappa_{sn} \sin nt\,, \tag{14}$$

Where n is the frequency of oscillation and $\varkappa_{cn}$ and $\varkappa_{sn}$ are Fourier coefficients.

In complex form, the solution to Eq. (4) is given by

$$u = \frac{\varkappa_0}{4v}\left(a^2 - r^2\right) - \sum_{n=1}^{\infty} \frac{i\varkappa_n}{n}\left[1 - \frac{J_o\left(kri^{\frac{3}{2}}\right)}{J_o\left(kai^{\frac{3}{2}}\right)}\right] e^{int} \tag{15}$$

Where

$$k = \sqrt{\frac{n}{v}} \tag{16}$$

The total mean velocity U is defined as $U = \frac{G}{\pi a^2}$, where G, the total mean mass flow, is given by

$$G = \frac{1}{2\pi}\int_0^{2\pi} dt \int_0^a 2\pi u r dr = \frac{\pi a^4 \varkappa_0}{8v}\,. \tag{17}$$

When this expression has been rearranged in order to introduce the mean pressure gradient, one gets

$$G = \frac{1}{2\pi}\int_0^{2\pi} dt \int_0^a 2\pi u r dr = \frac{\pi a^4 \varkappa_0}{8\mu}\overline{\left(-\frac{\partial p}{\partial x}\right)}, \tag{18}$$

Where $\overline{\left(-\frac{\partial p}{\partial x}\right)} = \rho\varkappa_0$, is the mean pressure gradient taken over time. Therefore,

$$U = \frac{a^2}{8\mu}\overline{\left(-\frac{\partial p}{\partial x}\right)}. \tag{19}$$

If one uses U as a velocity scale, the nondimensional expression of the velocity is given by

$$\frac{u}{U} = \frac{u_s}{U} + \frac{u'}{U} \tag{20}$$

with

$$\frac{u_s}{U} = 2\left(1 - \frac{r^2}{a^2}\right) \tag{21}$$

And

$$\frac{u'}{U} = \sum_{n=1}^{\infty} \frac{\varkappa_{cn}}{\varkappa_0}\left\{\frac{8B}{(ka)^2}cosnt + \frac{8(1-A)}{(ka)^2}sinnt\right\} + \sum_{n=1}^{\infty} \frac{\varkappa_{sn}}{\varkappa_0}\left\{\frac{8B}{(ka)^2}sinnt - \frac{8(1-A)}{(ka)^2}cosnt\right\},$$

where

$$A = \frac{ber(ka)ber(kr) + bei(ka)\ bei(kr)}{ber^2(ka) + bei^2(kr)}, \quad B = \frac{bei(ka)ber(kr) - ber(ka)\ bei(kr)}{ber^2(ka) + bei^2(kr)} \text{ (a)}$$

And

$$J_o\left(kri^{\frac{3}{2}}\right) = ber(kr) + ibei(kr) \text{ (b)} \tag{22}$$

In which *ber* and *bei* are Kelvin functions defined using infinite series as shown below:

$$ber(z) = \sum_{k=0}^{\infty} \frac{(-1)^k\left(\frac{z}{2}\right)^{4k}}{((2k)!)^2} \text{ (c)}$$

and

$$bei(z) = \sum_{k=0}^{\infty} \frac{(-1)^k\left(\frac{z}{2}\right)^{4k+2}}{((2k+1)!)^2} \text{ . (d)}$$

4.4. Asymptotic expressions of the velocity distribution

Two extreme cases were considered by Uchida: the case of very slow pulsations and that of very fast pulsations, depending on the magnitude of the dimensionless parameter $ka = \sqrt{\frac{n}{v}}a$

Consider very slow pulsations of the pressure gradients. If $= \sqrt{\frac{n}{v}}a \ll 1$, pulsations of the pressure gradients are very slow. Then, under these conditions and from the behavior of Kelvin functions, it is reasonable to expect that

$berka \to 1$ *and* $beika \to 0$.

Then, the velocity takes the form

$$\frac{u}{U} = 2\left(1 - \frac{r^2}{a^2}\right)\frac{1}{\varkappa_0}\left[-\frac{1}{\rho}\frac{\partial p}{\partial x}\right] = \frac{1}{4\mu}\left(a^2 - r^2\right)\left[-\frac{1}{\rho}\frac{\partial p}{\partial x}\right]. \tag{23}$$

In this case, the velocity distribution is a quadratic function of the radial distance from the axis of the pipe ; and the corresponding velocity profile is parabolic. This result is similar to

http://dx.doi.org/10.5772/54144

what is obtained in steady flow. However, the magnitude of the velocity is a periodic function of time and is always in phase with the driving pressure gradient.

Consider very fast pulsations of the pressure gradients. If $ka=\sqrt{\frac{n}{v}}a \to \infty$, pulsations of the pressure gradients are very fast. Then, Uchida used asymptotic expansions of ber(ka) and bei(ka). In this extreme, the expression for the velocity near the center of the pipe is different from that near the wall of the pipe. So, they are discussed separately.

Near the center of the pipe, $ka \to \infty$ *and* $kr \to 0$, one gets

$$\frac{u}{U}=\frac{\varkappa_0}{4v}\left(a^2-r^2\right)+\sum_{n=1}^{\infty}\frac{\varkappa_{cn}}{n}\cos\left(nt-\frac{\pi}{2}\right)+\sum_{n=1}^{\infty}\frac{\varkappa_{sn}}{n}\sin\left(nt-\frac{\pi}{2}\right). \tag{24}$$

Comparing this to Eq. (14), one sees that when the pulsations are very rapid, fluid near the axis of the pipe moves with a phase lag of 90° relative the driving pressure gradient and its amplitude decreases as the frequency of pulsation increases.

Near the wall of the pipe, $kr \to ka \to \infty$, and one uses asymptotic expansions of Bessel functions to get

$$\begin{aligned}\frac{u}{U}=&2\left(1-\frac{r^2}{a^2}\right)+\sum_{n=1}^{\infty}\frac{\varkappa_{cn}}{\varkappa_0}\frac{8}{(ka)^2}\left\{\sin(nt)-\sqrt{\frac{a}{r}}\exp\left(-\frac{k(a-r)}{\sqrt{2}}\right)\sin\left[nt-\frac{k(a-r)}{\sqrt{2}}\right]\right\}\\&+\sum_{n=1}^{\infty}\frac{\varkappa_{sn}}{\varkappa_0}\frac{8}{(ka)^2}\left\{-\cos(nt)+\sqrt{\frac{a}{r}}\exp\left(-\frac{k(a-r)}{\sqrt{2}}\right)\cos\left[nt-\frac{k(a-r)}{\sqrt{2}}\right]\right\}.\end{aligned} \tag{25}$$

4.5. Case of a general periodic pressure gradient: Graphical illustrations of Uchida's results

Uchida presented graphical illustrations of these results for four different values of the parameter ka: 1, 3, 5, and 10.

At each value of the parameter ka and using the angle, nt, as the variable, he plotted twelve different snapshots of the velocity profiles of the unsteady component of velocity for the following angles:

$nt = 0^0,\ 30^0,\ 60^0,\ 90^0,\ 120^0,\ 150^0,\ 180^0,\ 210^0,\ 240^0,\ 270^0,\ 300^0,\ 330^0$.

His plots showed that, as the value of ka was increased, the location of maximum velocities shifted progressively away from the axis of the pipe and moved towards the wall. At ka = 1, all maximums of velocity distributions occurred on the axis of the pipe. At ka = 3, two maximums of velocity distributions had shifted away from the axis and moved toward the wall of the pipe. These occurred at nt = 0° and nt = 180°. At ka = 5, half the maximums of velocity distributions had shifted away from the axis and moved toward the wall of the pipe. These occurred at nt = 0°, 30 °, 60 °, 180 °, 210 ° and 240 °. At ka = 10, all of the maximums of velocity

distributions had shifted away from the axis and occurred by the wall of the pipe. These results are summarized in Table 1 and Uchida's (1956) plots are reproduced in enlarged formats in Figures 5(a), 5(b), 6(a), and 6(b), as shown below.

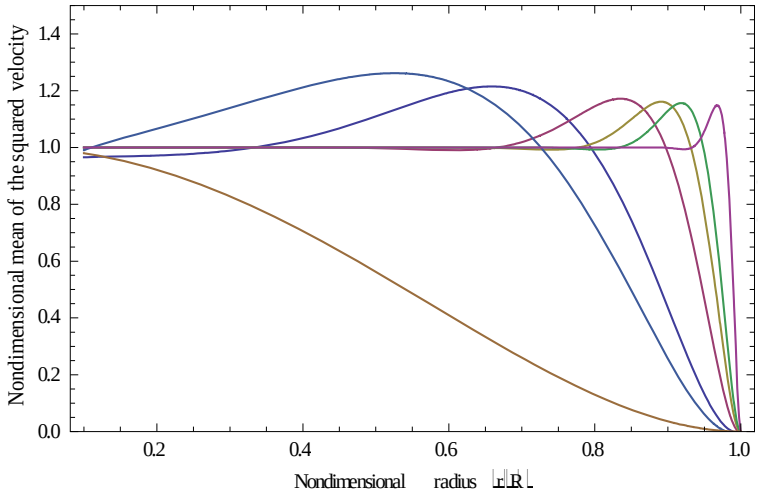

Figure 4. As the frequency of pressure pulsations increases, the point of maximum velocity shifts progressively away from the axis of the pipe and moves towards its wall (plots of Eq. (2), for increasing values of n).

ka	Total maximums	Maximums on the axis of the pipe	Maximums away from the axis of the pipe
1	12	12	0
3	12	10	2
5	12	6	6
10	12	0	12

Table 1. Data extracted from Uchida's papers (his Figures 1, 2, 3, and 4 are shown below).

5. Pulsating flow through rectangular ducts

5.1. Summary of the results of analysis

Yakhot, Arad, and Ben-dor conducted numerical studies of pulsating flows in very long rectangular ducts, where a and h were the horizontal and the vertical dimensions, respectively, of the cross-section of the duct, Fig. 7. Letting $\alpha = \left(\frac{\omega}{2\upsilon}\right)^{1/2}$, they performed calculations for low and high frequency regimes ($1 \leq \alpha h \leq 20$) in rectangular ducts using two different as-

http://dx.doi.org/10.5772/54144

pect ratios (a/h =1 and a/h = 10). They presented results for low frequencies (αh =1) and moderate frequencies (αh =8). They indicated that results for frequencies higher, $\alpha h \geq 10$, were very similar to those for moderate frequencies. The other conclusions that they came up with are summarized below.

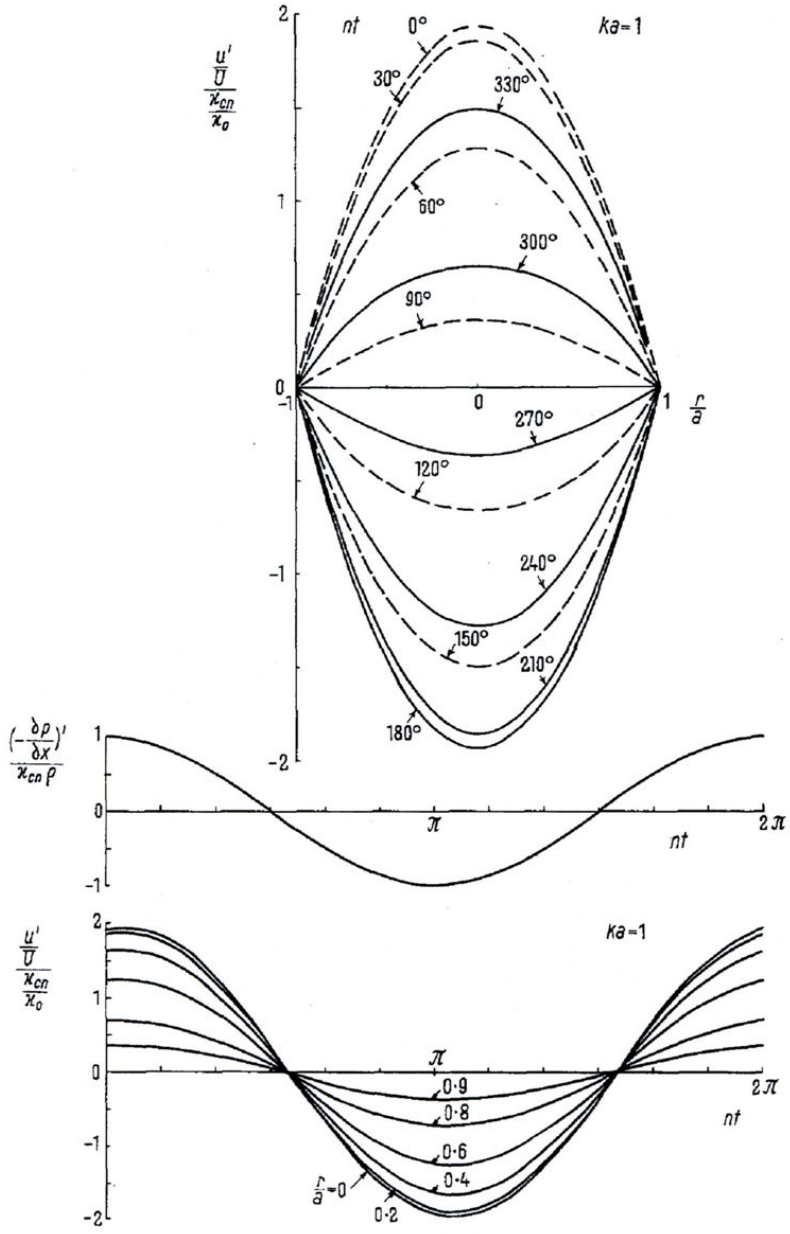
nt
0°
ka=1
30°
330°
60°
300°
90°
270°
120°
240°
150°
210°
180°
r/a
nt
ka=1
0·9
0·8
0·6
0·4
0·2
r/a=0

http://dx.doi.org/10.5772/54144

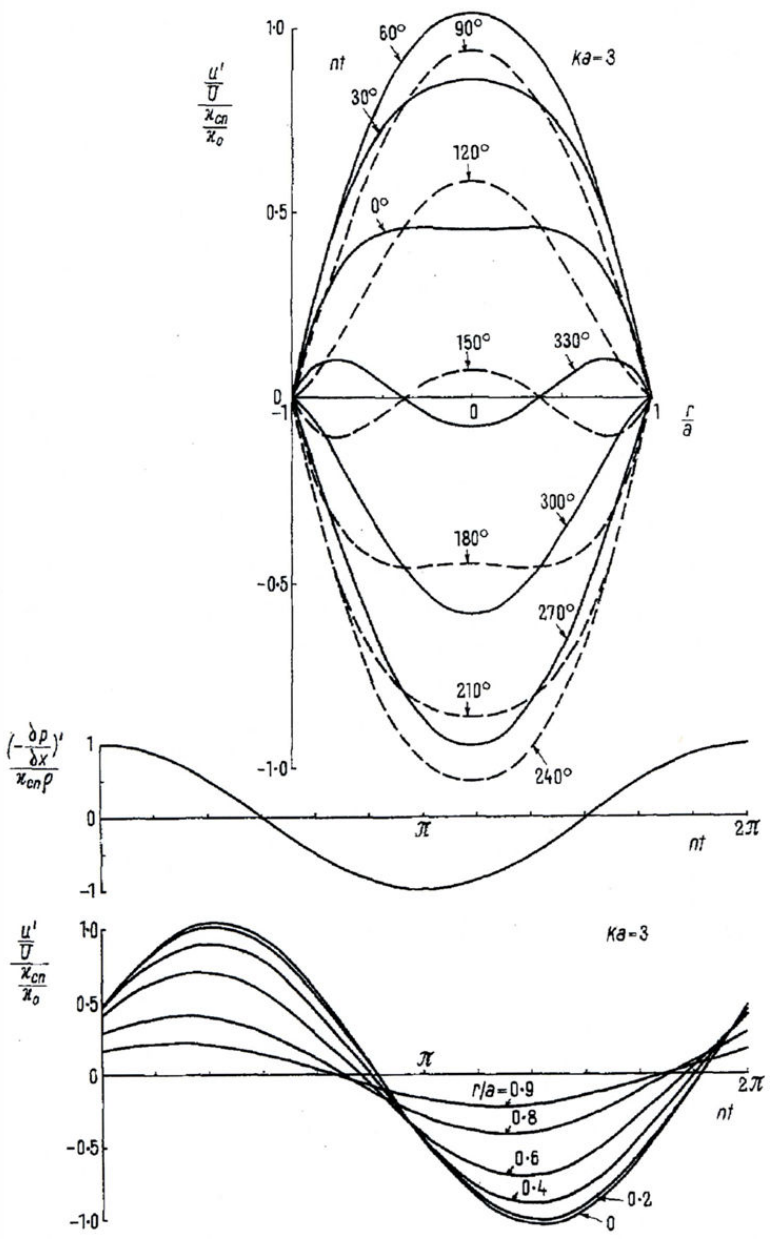

Figure 5. (a). Where maximums of velocity distributions occur when the parameter ka = 1. The angle nt is the parameter; in these plots, $nt = 0^0$, 30^0, 60^0, 90^0, 120^0, 150^0, 180^0, 210^0, 240^0, 270^0, 300^0, 330^0. (b). Where maximums of velocity distributions occur when the parameter ka = 3. The angle nt is the parameter; in these plots, $nt = 0^0$, 30^0, 60^0, 90^0, 120^0, 150^0, 180^0, 210^0, 240^0, 270^0, 300^0, 330^0.

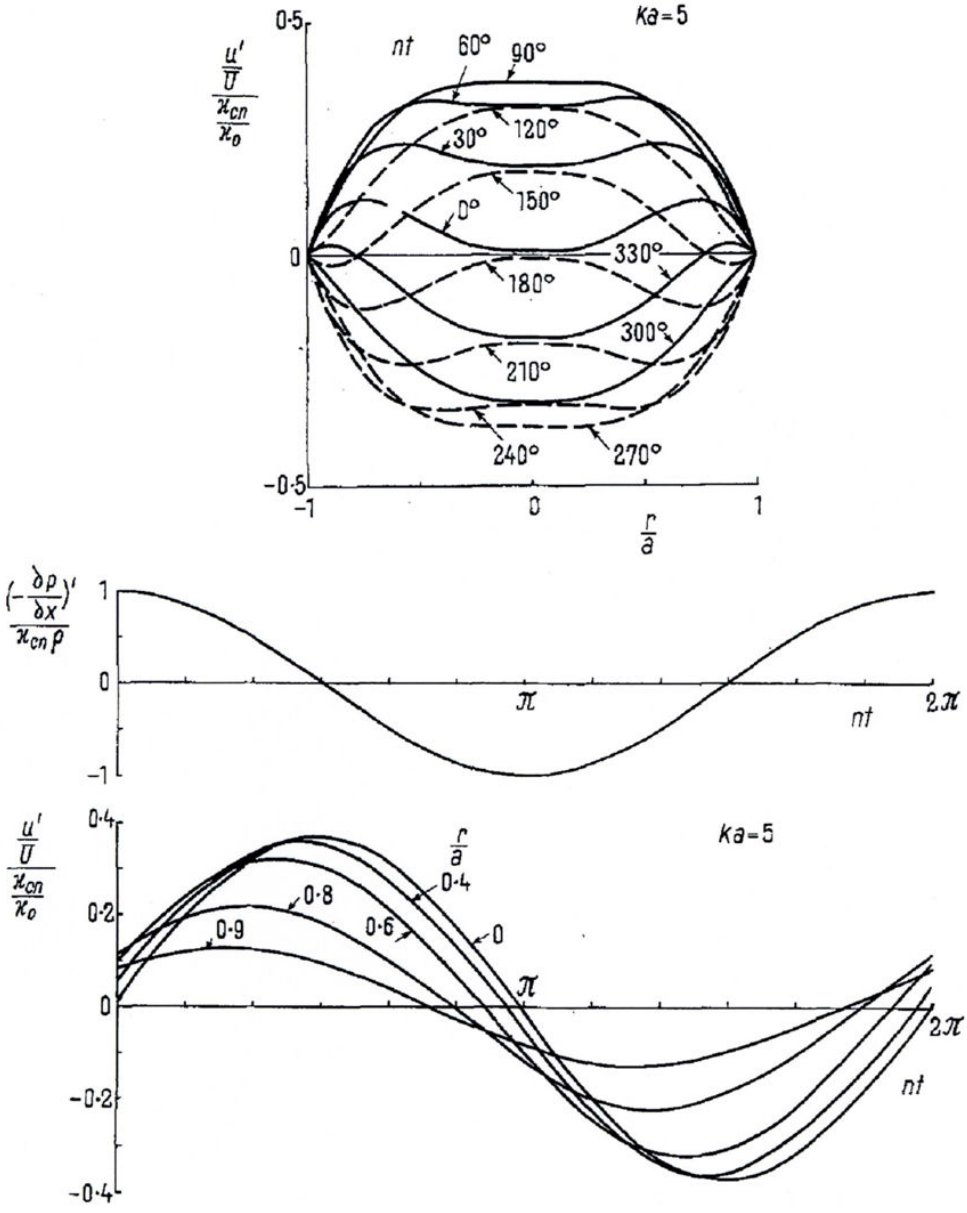
Ka=5
nt
60°
90°
30°
120°
0°
150°
330°
180°
300°
210°
240°
270°
0·5
0
-0·5
-1
1
r/a
u'/U / κcn/κo
(-∂p/∂x)' / κcn ρ
π
2π
nt
Ka=5
0·4
0·2
-0·2
-0·4
0·8
0·9
0·6

http://dx.doi.org/10.5772/54144

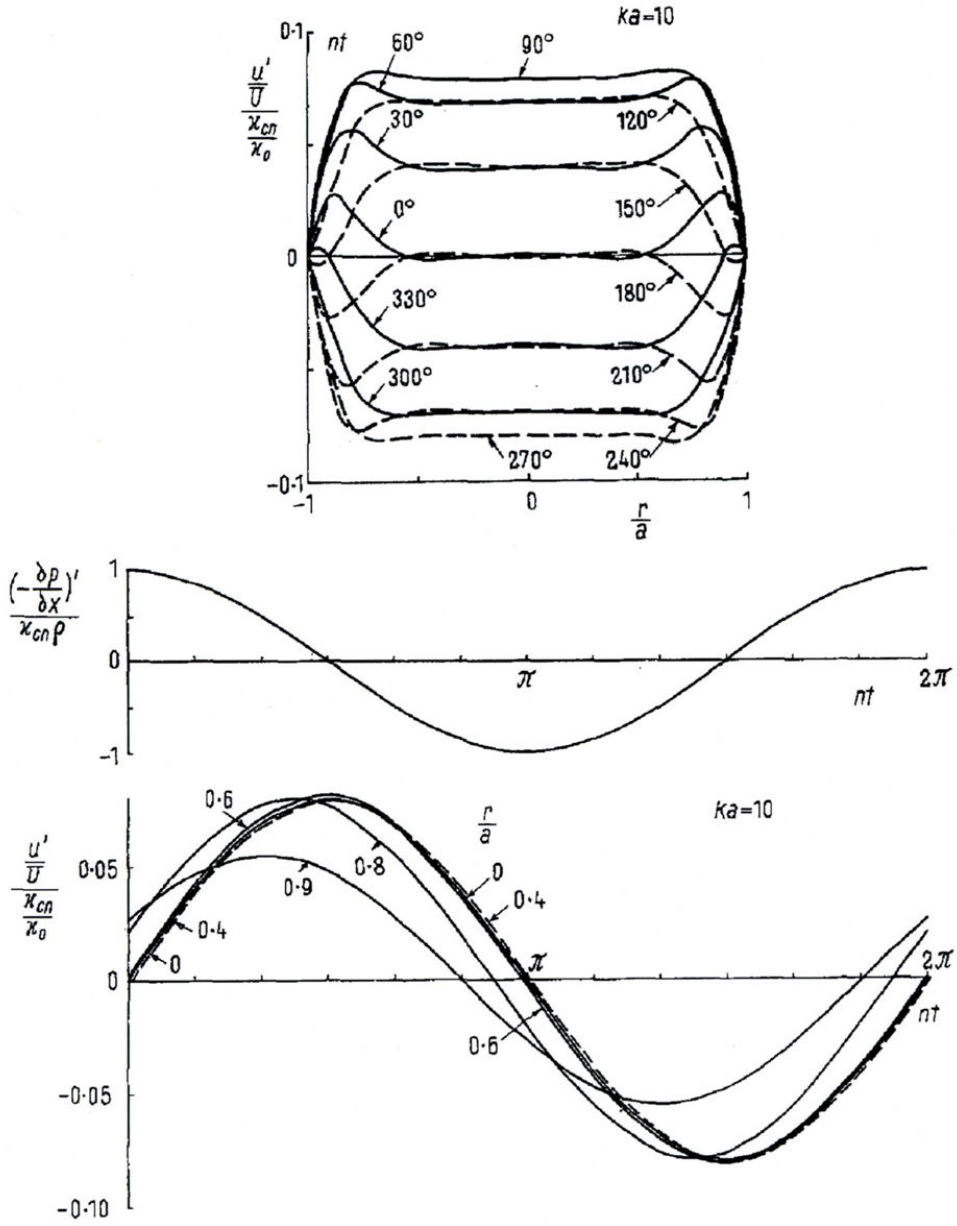

Figure 6. (a) Where maximums of velocity distributions occur when the parameter ka = 5. The angle nt is the parameter; *intheseplots*, $nt = 0^0$, 30^0, 60^0, 90^0, 120^0, 150^0, 180^0, 210^0, 240^0, 270^0, 300^0, 330^0. (b). Where maximums of velocity distributions occur when the parameter ka = 10. The angle nt is the parameter; *in these plots*, $nt = 0^0$, 30^0, 60^0, 90^0, 120^0, 150^0, 180^0, 210^0, 240^0, 270^0, 300^0, 330^0.

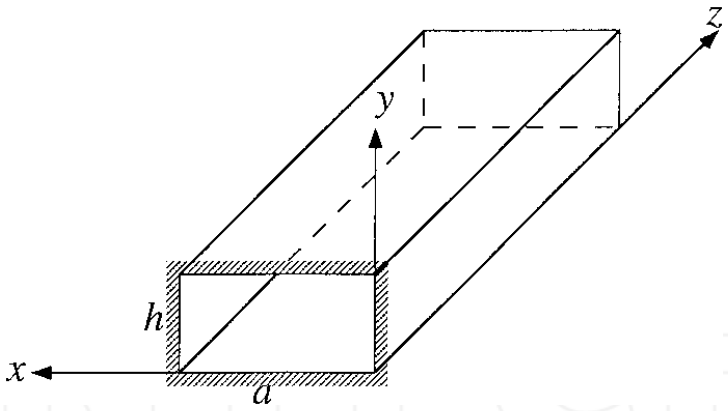

Figure 7. Sketch of the rectangular duct used by Yakhot, Arad and Ben-dor (1999) in their numerical studies.

For low pulsating frequencies, h =1 , flow in a duct of square cross-sectional area, the velocity distribution is in phase, that is in lock step, with the driving pressure gradient. This was true at low and at high aspect ratios. This result is the same as what happens in the case of flow between parallel plates. When one compares the amplitudes of the induced velocity, one finds that the amplitude of flow between flat plates is larger than that in a square duct. This is due to the fact that, in a duct the fluid experiences friction of four sides, whereas in the case of flow between parallel plates, it experiences flow only from two sides. When the aspect ratio is increased to a/h = 10, the velocity in the duct differs only with the velocity between parallel plates near the side walls. This is clearly due to the effects of viscosity.

For moderately pulsating frequencies, αh =8 , the velocity distribution of the flow in a duct of square cross- sectional area differs considerably from that obtained at low frequencies. The shapes of the velocity profiles are different; results indicate that, at certain instants of time during a complete cycle, the profiles reach maximum values near the wall of the pipe rather than on its axis of symmetry. This is Richardson's "annular effect". The induced velocity is no longer in phase, that is in lock step, with the driving pressure gradient. Rather, the velocity is shifted with respect to the driving pressure and the magnitude of the shift depends on how far away points in the flow space are from the wall. Near the wall, the induced velocity on the axis of the duct lags behind that in the regions that are near the walls of the duct. On the axis, the phase shift is 90^o. This was true at low and at high aspect ratios. This result is the same as what happens in the case of flow between parallel plates. When one compares the amplitudes of the induced velocity, one finds that the amplitude of flow between flat plates is larger than that in a square duct. This is due to the fact that, in a duct the fluid experiences friction of four sides, whereas in the case of flow between parallel plates, it experiences flow only from two sides. When the aspect ratio is increased to a/h = 10, the velocity in the duct differs only with the velocity between parallel plates near the side walls. This is clearly due to the effects of viscosity.

http://dx.doi.org/10.5772/54144

5.2. Graphical illustration of the results of analysis by Yakhot, Arad and Ben-dor (1999)

The velocity profiles in pulsating flow at selected instants within one complete period are shown below. Flow in a duct is compared to flow between parallel plates for different aspect ratios and frequencies.

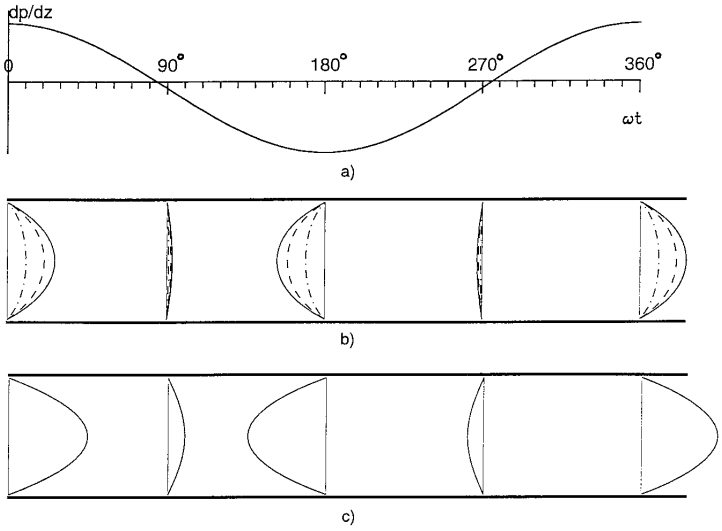

Figure 8. Velocity profiles in pulsating flow at different instants of one period. (a) Pressure gradient variation with time. (b) Duct flow, a/*h* =1, *α h =1*: solid line, *x*/*a* = 0.5; dashed, *x*/*a* = 0.25; dot-dashed, *x*/*a* = 0.1. (c) Flow between two parallel plates.

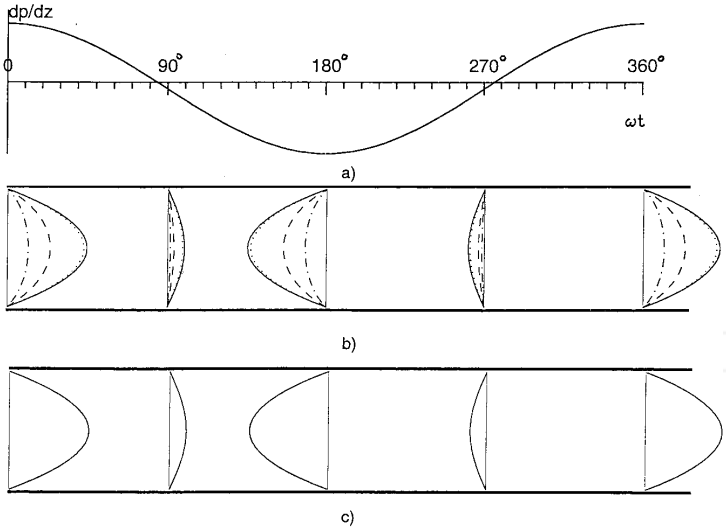

Figure 9. Velocity profiles in pulsating flow at different instants of one period. (a) Pressure gradient variation with time. (b) Duct flow, a/*h* =10, *α h=1*: solid line, *x*/*a* = 0.5; dot, *x*/*a* = 0.1; dashed, *x*/*a* = 0.025; dot-dashed, *x*/*a* = 0.01. (c) Flow between two parallel plates.

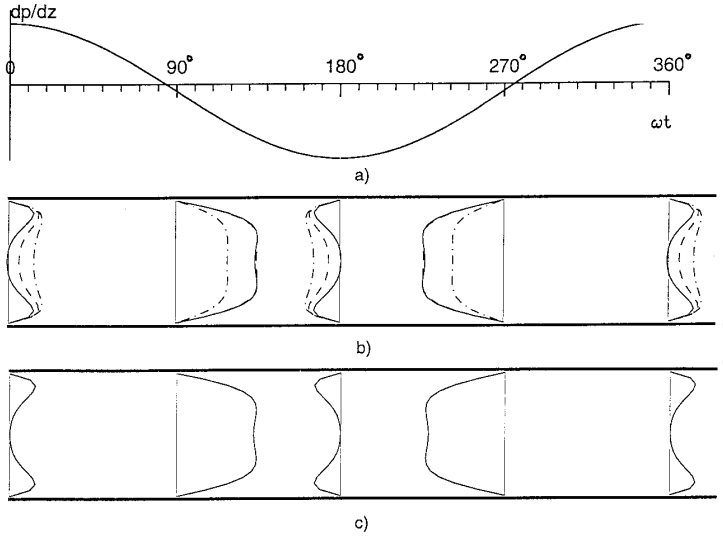

Figure 10. Velocity profiles in pulsating flow at different instants of one period. (a) Pressure gradient variation with time. (b) Duct flow, a/*h* =1, *α h=8*: solid line, *x*/*a* = 0.5; dashed, *x*/*a* = 0.25; dot-dashed, *x*/*a* = 0.1. (c) Flow between two parallel plates.

http://dx.doi.org/10.5772/54144

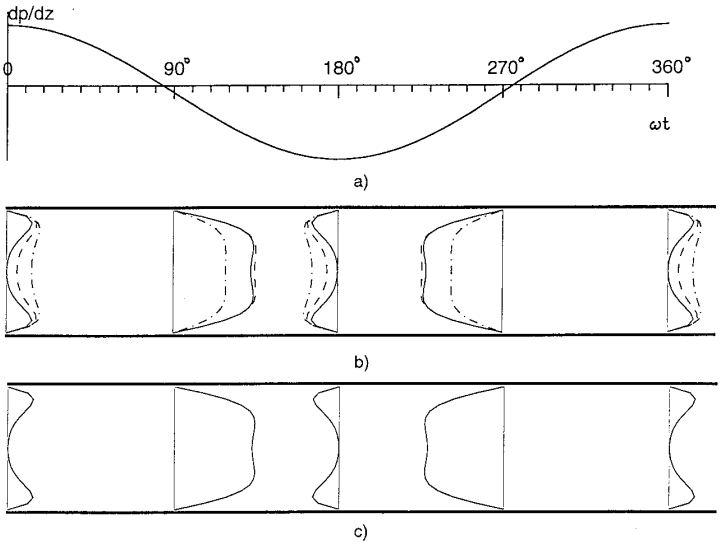

Figure 11. Velocity profiles in pulsating flow at different instants of one period. (a) Pressure gradient variation with time. (b) Duct flow, a/*h* =10, *a h=8*: solid line, *x*/*a* = 0.5; dashed, *x*/*a* = 0.025; dot-dashed, *x*/*a* = 0.01. (c) Flow between two parallel plates.

6. Anatomy of the shift using expansions of general results into power series

6.1. Series expansions of Kelvin functions

The unsteady part of the solution, which is given by $\frac{u'}{U}$, Eq. (22), can be written to show the pressure gradient explicitly as shown below.

$$\frac{u'}{U}=\sum_{n=1}^{\infty} W\left(r,\, a,\, k\right)\left\{\frac{\varkappa_{cn}}{\varkappa_0}cos(nt-\varphi)+\frac{\varkappa_{sn}}{\varkappa_0}sin(nt-\varphi)\right\} \tag{26}$$

Where

$$W(r,\, a,\, k)=\frac{8B}{(ka)^2}\left[B^2+(1-A)^2\right]^{1/2} \tag{27}$$

And $tan(\varphi(r,\, a,\, k))=\frac{1-A}{B}$

After a considerable amount of algebra using series expansions for the ber and bei functions, it can be shown that

$$W(r, a, k) = 2\left(1 - \frac{r^2}{a^2}\right) D(r, a, k) \tag{28}$$

Where D(r, a, k) is a dimensionless factor that is defined as shown below

$$D(r, a, k) = \left\{ \frac{\sum_{n'=0}^{\infty} F_m(x, y)}{(ber^2 ka + bei^2 ka)} \right\}^{1/2} \tag{29}$$

Where m = 4n', with n' = 0,1,2,3,…, $x = ka$, $y = \frac{r}{a}$, and $F_m(x, y)$ denotes a family of polynomials a sample of which is shown below

$$F_0 = 1 \tag{30}$$

$$F_4 = \frac{4}{(4!)^2}\left(\frac{x}{2}\right)^4 \left(1 + 10y^2 + y^4\right)$$

$$F_8 = \frac{22}{(6!)^2}\left(\frac{x}{2}\right)^8 \left(1 - \frac{14}{11}y^2 + \frac{186}{11}y^4 - \frac{14}{11}y^6 + y^8\right)$$

$$F_{12} = \frac{68}{(8!)^2}\left(\frac{x}{2}\right)^{12} \left(1 + \frac{66}{17}y^2 - \frac{277}{17}y^4 + \frac{948}{17}y^6 - \frac{277}{17}y^8 + \frac{66}{17}y^{10} + y^{12}\right)$$

$$F_{16} = \frac{254}{(10!)^2}\left(\frac{x}{2}\right)^{16} \left(1 + \frac{154}{127}y^2 + \frac{2206}{127}y^4 - \frac{10142}{127}y^6 + \frac{21610}{127}y^8 - \frac{10142}{127}y^{10} + \frac{2206}{127}y^{12} + \frac{154}{127}y^{14} + y^{16}\right)$$

$$F_{20} = \frac{922}{(12!)^2}\left(\frac{x}{2}\right)^{20} \left(1 + \frac{1066}{461}y^2 - \frac{2685}{461}y^4 + \frac{41964}{461}y^6 - \frac{158412}{461}y^8 + \frac{268476}{461}y^{10} - \frac{158412}{461}y^{12} + \frac{41964}{461}y^{14} - \frac{2685}{461}y^{16} + \frac{1066}{461}y^{18} + y^{20}\right)$$

$$F_{24} = \frac{3434}{(14!)^2}\left(\frac{x}{2}\right)^{24} \left(\begin{array}{l} 1 + \frac{3238}{1717}y^2 + \frac{13040}{1717}y^4 - \frac{109654}{1717}y^6 + \frac{769653}{1717}y^8 - \frac{2359044}{1717}y^{10} + \frac{3530268}{1717}y^{12} - \\ - \frac{2359044}{1717}y^{14} + \frac{769653}{1717}y^{16} - \frac{109654}{1717}y^{18} + \frac{13040}{1717}y^{20} + \frac{3238}{1717}y^{22} + y^{24} \end{array}\right)$$

$$F_{28} = \frac{12868}{(16!)^2}\left(\frac{x}{2}\right)^{28} \left(\begin{array}{l} 1 + \frac{25992}{12868}y^2 + \frac{24716}{12868}y^4 + \frac{337040}{12868}y^6 - \frac{2663036}{12868}y^8 + \frac{13416312}{12868}y^{10} - \frac{34632404}{12868}y^{12} + \frac{48192480}{12868}y^{14} - \\ - \frac{34632404}{12868}y^{16} + \frac{13416312}{12868}y^{18} - \frac{2663036}{12868}y^{20} + \frac{337040}{12868}y^{22} + \frac{24716}{12868}y^{24} + \frac{25992}{12868}y^{26} + y^{28} \end{array}\right)$$

Note, from the definition of w(r, a, k), Eq. (28), that each of these polynomials will be multiplied by the steady velocity. Clearly, this shows that all components that are added to the velocity due to unsteadiness are essentially various forms of the same steady velocity after it has been modified by the introduction of time variations. The series of equations shown below demonstrates this observation:

$$\frac{u}{U} = \frac{u_s}{U} + \frac{u'}{U}, \tag{31}$$

$$\frac{u_s}{U} = 2\left(1 - \frac{r^2}{a^2}\right), \tag{32}$$

http://dx.doi.org/10.5772/54144

$$\frac{u}{U} = 2\left(1 - \frac{r^2}{a^2}\right) + \sum_{n=1}^{\infty} W\left(r, a, k\right)\left\{\frac{\varkappa_{cn}}{\varkappa_0} cos(nt - \varphi) + \frac{\varkappa_{sn}}{\varkappa_0} sin(nt - \varphi)\right\}, \tag{33}$$

Using the expression for $W(r, a, k)$ that is shown in Eq. (28), one gets

$$\frac{u}{U} = 2\left(1 - \frac{r^2}{a^2}\right) + 2\left(1 - \frac{r^2}{a^2}\right)\sum_{n=1}^{\infty} D\left(r, a, k\right)\left\{\frac{\varkappa_{cn}}{\varkappa_0} cos(nt - \varphi) + \frac{\varkappa_{sn}}{\varkappa_0} sin(nt - \varphi)\right\}, \tag{34}$$

After a minor rearrangement of terms, Eq. (34) becomes

$$\frac{u}{U} = 2\left(1 - \frac{r^2}{a^2}\right) + 2\left(1 - \frac{r^2}{a^2}\right)\sum_{n=1}^{\infty} \frac{D(r, a, k)}{\varkappa_0}\{\varkappa_{cn} cos(nt - \varphi) + \varkappa_{sn} sin(nt - \varphi)\}. \tag{35}$$

Since D(r, a, k), in Eq. (35), consists of the functions $F_m(x, y)$, one concludes that the family of polynomials $F_m(x, y)$ that is shown in Eq.(30) is what is primarily responsible for the change in the shape of the velocity profile as the frequency of oscillation increases. Therefore, it is those polynomials that cause the location of the maximum velocity to move away from the axis of the pipe, and hence, bear the essence of the physical interaction between viscous forces and pressure forces during pulsating motions. This conclusion will be illustrated graphically below.

6.2. Graphical illustrations of the shape of the $F_m(x, y)$ polynomials

Variation in the shapes of the functions $F_m(x, y)$ is illustrated graphically below. It will be remembered that, in what follows, $x = ka = \sqrt{\frac{n}{v}}a$, y = $\frac{r}{a}$, the dimensionless radial distance from the axis of the pipe; and that

m = 4n′, with n′ = 1, 2, 3, 4, 5, … In Figures 12 and 13, twelve functions $F_m(x, y)$ are plotted against the radial distance y for various values of the dimensionless parameter x.

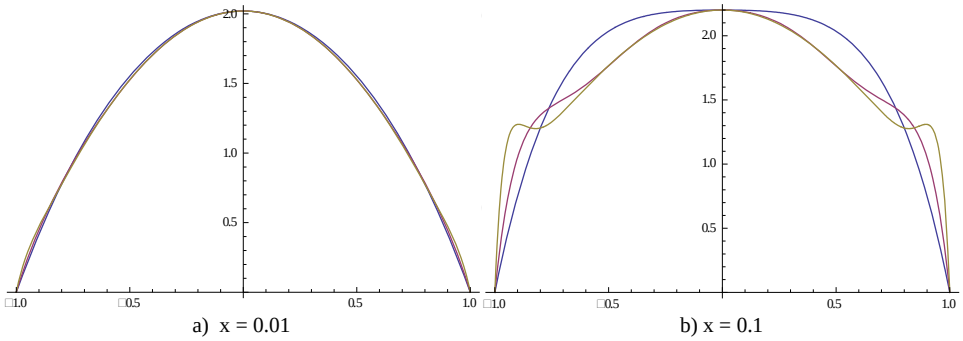

Figure 12. Each coordinate frame shows plots of three functions $F_m(x, y)$ vs y: $F_4(x, y)$, $F_{12}(x, y)$, and $F_{28}(x, y)$; x is used as the parameter. Note that larger values of x indicate higher rates of pulsations by the pressure gradient.

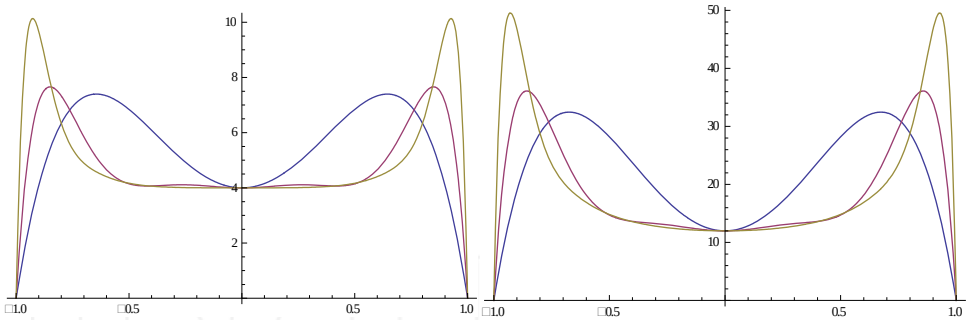

Figure 13. Each coordinate frame shows plots of three functions $F_m(x, y)$ vs. y: $F_4(x, y)$, $F_{12}(x, y)$, and $F_{28}(x, y)$; x is the parameter. Note that larger values of x indicate higher rates of pulsations by the pressure gradient.

7. Compiled summary of results from several investigators and conclusions

While conducting experiment on sound waves in resonators, Richardson (1928) measured velocities across an orifice of circular cross-section and found that the maximum velocity could occur away from the axis of symmetry and toward the wall. Sexl (1930) proved analytically that what Richardson observed could happen. Richardson and Tyler (1929-1930) confirmed these findings with more experiments with a pure periodic flow generated by the reciprocating motion of a piston. Uchida (1956) studied the case of periodic motions that were superposed upon a steady Poiseuille flow. An exact solution for the pulsating laminar flow that is superposed on the steady motion in a circular pipe was presented by Uchida (1956) under the assumption that that flow was parallel to the axis of the pipe.

The total mean mass of flow in pulsating motion was found to be identical to that given by Hagen-Poiseuille's law when the steady pressure gradient used in the Hagen-Poiseuille's law was equal to the mean pressure gradient to which the pulsating flow was subjected.

The phase lag of the velocity variation from that of the pressure gradient increases from zero in the steady flow to 90° in the pulsation of infinite frequency.

Integration of the work needed for changing the kinetic energy of fluid over a complete cycle yields zero, however, a similar integration of the dissipation of energy by internal friction remains finite and an excess amount caused by the components of periodic motion is added to what is generated by the steady flow alone.

It follows that a given rate of mass flow can be attained in pulsating motion by giving the same amount of average gradient of pressure as in steady flow. However, in order to maintain this motion in pulsating flow, extra work is necessary over and above what is required when the flow is steady.

http://dx.doi.org/10.5772/54144

Recently, Camacho, Martinez, and Rendon (2012) showed that the location of the characteristic overshoot of the Richardson's annular effect changes with the kinematic Reynolds number in the range of frequencies within the laminar regime. They identified the existence of transverse damped waves that are similar to those observed in Stokes' second problem.

All these results were obtained in flows through pipes of circular cross-sections and rectangular ducts. It is reasonable to expect that they would hold in the flow of air in a wind tunnel. Experimental results indicate that the Richardson's annular effect does occur in the test section of a subsonic wind tunnel. That behavior first appears unusual and, indeed, odd. However, as shown in this chapter, there is considerable experimental and analytical evidence in the literature that indicates that this behavior is due to high-frequency pulsations of the pressure gradient. Accordingly, in the case of a subsonic wind tunnel, it is probably due to the fast rate of rotation of fan blades. Indeed, in our wind tunnel, results from analysis and those from experiments differed only by about 5.7%.

Nomenclature of the symbols (with units)

α : a dimensionless ratio that combines the rate of pressure pulsations and the distance from the wall of the pipe;

η : a dimensionless distance from the wall of the pipe;

ρ : the mass density of the fluid (kg/m^3);

μ : the coefficient of absolute viscosity (N.s/ m^2);

v : the coefficient of kinematic viscosity (m^2/s);

ω : denotes the circular frequency of pressure oscillations;

$\varkappa_{cn}$ and $\varkappa_{sn}$: Fourier coefficients of the pressure gradient; $\varkappa_o$ is the steady part of the pressure gradient (m/s^2);

a: the inside radius of a pipe through which an oscillating flow is moving;

c : the magnitude of a reference speed

G: the total mean value of the mass flow, U the total mean value of the velocity

i : the pure imaginary number; it is defined by $i^2 = -1$

J_o : Bessel function of the first kind and of zero order

k: a dimensionless ratio used by Schlichting to denote the magnitude of the frequency of oscillation

K: a symbol used by Schlichting to indicate the magnitude of the pressure gradient

n: denotes the circular frequency of pressure oscillations (rad/s)

P: the pressure that drives the flow (N/m^2)

$\frac{\partial p}{\partial x}$: the pressure gradient in the axial direction of an infinitely long pipe

r: the radial distance measured from the axis of the pipe (m)

R: the inside radius of a pipe of circular cross section (m)

t: time elapsed (s)

u: the axial velocity of the flow (m/s)

u_s: the steady part of the velocity u (m/s)

u' : the unsteady part of the velocity u (m/s

U : the mean speed (m/s) of the velocity u (m/s)

x: a dimensionless ratio that measures the rate of pulsations of the pressure gradient

y: a dimensional distance from the wall of the pipe (m)

Author details

Josué Njock Libii

Indiana University-Purdue University Fort Wayne, Fort Wayne, Indiana, USA

References

[1] Richardson, E.G. and Tyler, E. (1929). The transverse velocity gradients near the mouths of pipes in which an alternating or continuous flow of air is established. The Proceedings of the Physical Society, Vol. 42, part I, No. 231, pp. 1-15. ISSN 0370-1328.

[2] Ury, Josef F. (1964), A graphical method for a closer study of Richardson's annular effect, Zeitschrift fur angewandteMathematik und Physik (ZAMP) 15, number 3, pp. 306-311. ISBN/ISSN: 1420-9039 OCLC:43807374.

[3] Camacho, F.J.; Martinez, R.; Rendon, L. (2012) The Richardson's Annular effect and a transient solution of oscillating pressure-driven flow in circular pipes, eprint arXiv: 1207.1495.

[4] Sexl, T. (1930). Uber die von E. G. Richardson entdecktenAnnuraleffekt.Zeitschrift fur Physik, 61, 349-62. ISBN 0691114390.

[5] Uchida, S. (1956). The Pulsating viscous flow superposed on the steady laminar motion of incompressible fluid in a circular pipe. Zeitschrift fur angewandteMathematik und Physik 7, 403-422. ISBN/ISSN: 1420-9039 OCLC:43807374.

http://dx.doi.org/10.5772/54144

[6] Yakhot, A. Arad, M., and Ben-dor, G.(1999), Numerical investigation of a laminar pulsating flow in a rectangular duct, International Journal for Numerical Methods in Fluids, Vol. 29, Issue 8, pp 899-996, 30 April 1999. ISSN 0271-2091.

[7] NjockLibii, J. (2010) Laboratory exercises to study viscous boundary layers in the testsection of an open-circuit wind tunnel, *World Transactions on Engineering and Technology Education(WTE&TE),* Vol. 8, No. 1, (March 2010), pp. (91-97), ISSN 1446-2257.

[8] JosuéNjockLibii (2011), Wind Tunnels in Engineering Education, in Wind Tunnels and Experimental Fluid Dynamics Research, Jorge Colman Lerner, UlfilasBoldes, editors, Chapter 11, InTech Publishers, 2011. ISBN 978-953-307-623-2.

[9] Yakhot, A., M. Arad, M., & Ben-Dor, G. (1998).Richardson's Annular Effect in Oscillating Laminar Duct Flows.*Journal of Fluids Engineering*, Vol. 120, 1, (March 1998) pp. (209-301), ISSN 0098-2202.

[10] Watson, G.N., (1944), A treatise on the theory of Bessel functions, Cambridge University Press, Cambridge, England, ISBN-10: 0521483913 | ISBN-13: 978-0521483919.

INTECH